Journal of Catalysis 283 (2011) 68–74

Contents lists available at SciVerse ScienceDirect

Journal of Catalysis

journal homepage: www.elsevier.com/locate/jcat

Catalytic role of different pore systems in MCM-49 zeolite for liquid alkylation of benzene with ethylene

Kefeng Liu [a,b], Sujuan Xie [a], Shenglin Liu [a], Guoliang Xu [a], Ningning Gao [a,b], Longya Xu [a,*]

[a] State Key Laboratory of Catalysis, Dalian Institute of Chemical Physics, Chinese Academy of Sciences, Dalian 116023, PR China
[b] Graduate University of Chinese Academy of Science, Beijing 100049, PR China

ARTICLE INFO

Article history:
Received 6 May 2011
Revised 4 July 2011
Accepted 8 July 2011
Available online 30 August 2011

Keywords:
MCM-49 zeolite
Liquid alkylation
Benzene
Ethylene
Pore system

ABSTRACT

The properties of three types of pore systems in MCM-49 zeolite have been investigated by precoking to block the supercages and poisoning the surface pockets. Most Lewis acid sites (ca. 73%) are located within the supercages, while 38% of Brönsted acid sites are located in the surface pockets, 28% in the sinusoidal pores and only 34% in the supercages, respectively. Alkylation of benzene with ethylene mainly occurs in the surface pockets, and the contribution from the sinusoidal pores is limited. The generation of heavy aromatics in supercages results in the deactivation of MCM-49 at the early reaction stage. A moderate alkali-treatment process has been demonstrated to enlarge the opening of supercages without affecting the sinusoidal pores, resulting in improved diffusion of big molecules and hence better catalytic performance for liquid alkylation of benzene with ethylene.

1. Introduction

Zeolites have been widely used in the petrochemical processes because of their unique advantages of highly selective, less toxic, environmentally friendly and readily reproducible in catalytic reactions [1]. The morphology, textural properties and chemical composition of zeolites significantly affect their catalytic performances. It is well known that many zeolites contain two or more kinds of pore systems. The nature and amounts of the acid sites vary in different pore systems, or even in the same type of pore in zeolites with different chemical compositions (Si/Al molar ratio), leading to diverse and sometimes conflicting results for the same catalytic reaction [2–5]. A number of methods, such as selective ion exchange [6] and poisoning by basic molecule adsorption [7,8], have been attempted to investigate the roles of acid sites in different locations or with different strengths in catalytic reactions. These results indicate that the acidity of zeolite can be tuned to some extent to favor the formation of targeted products.

Liquid alkylation of benzene with ethylene is an important petrochemical process to produce ethylbenzene. Some zeolites, such as USY, Beta and MCM-22, exhibit promising performance in this reaction [1,9–11]. Especially MCM-22 zeolite attracts remarkable attention due to the higher selectivity of ethylbenzene [10]. This has been attributed to its special pore systems: the two-dimensional sinusoidal 10 membered ring (MR) pore (0.41 × 0.51 nm) and the large cylindrical supercage defined by 12MR (0.71 nm o.d. × 1.82 nm height) with 10MR opening (0.41 × 0.54 nm). Furthermore, there are half-supercages (denoted as surface pocket) scattering over the surface (0.71 nm o.d. × 0.90 nm height) [12,13]. The acid sites in the pockets of MCM-22 zeolite can be characterized by poisoning method with bulky alkaline molecules like di-tert-butylpyridine [14], collidine [15] and 2,6-dimethylquinoline [8,16]. Moreover, the supercage pore system of MCM-22 can be selectively blocked by precoking through the *m*-xylene transformation [17–19]. Therefore, the identification of the acid sites in three different pore systems (pocket, supercage and sinusoidal pore) of MCM-22 has been realized, paving the path for the studies of their roles in catalytic reactions. Although MCM-49 zeolite possesses nearly the same framework topology as the calcinated MCM-22 (only the average unit cell *c*-parameter is ~0.02 nm longer in MCM-49) [20], it is noted that MCM-49 zeolite exhibits much higher selectivity of ethylbenzene in the alkylation of benzene with ethylene [21]. Therefore, it is important to investigate the effect of acid properties and pore structures of MCM-49 zeolite on the liquid alkylation of benzene with ethylene.

In this work, we have studied the roles of different pore systems in MCM-49 zeolite (pocket, supercage and sinusoidal pore) for the liquid alkylation of benzene with ethylene. Possible reaction pathways in different pore systems are proposed. Furthermore, the effects of alkali treatment on different pore systems of MCM-49 have been studied to elucidate the primary cause of the improved catalytic performance for the alkylation of benzene.

* Corresponding author. Fax: +86 411 84693292.
E-mail address: lyxu@dicp.ac.cn (L. Xu).

0021-9517/$ - see front matter © 2011 Elsevier Inc. All rights reserved.
doi:10.1016/j.jcat.2011.07.004

2. Experimental

2.1. Catalyst preparation

The as-received Na-MCM-49 zeolite (Si/Al molar ratio of 10.2, Tieling Catalyst) was calcinated at 540 °C for 6 h to remove the template, followed by three repeated ion exchanges in 0.8 N NH_4NO_3 solution at 80 °C for 2 h. H-form MCM-49 zeolites was obtained by the calcination of its NH_4^+ form counterpart, and the sample was named as HM. The alkali-treated samples were prepared in the NaOH solutions with different concentrations at the given temperatures for a certain period and transformed into H-form. The resulting samples were denoted as 0.025AT (0.025 N NaOH solution, 25 °C and 15 min) and 0.3AT (0.3 N NaOH solution, 75 °C and 120 min), respectively. All the H-form samples were pressed into tablets, crushed and sieved into 20–40 mesh particles.

Samples with the precoked supercages, denoted as HM_{xy}, $0.025AT_{xy}$ and $0.3AT_{xy}$ respectively, were prepared following a reported procedure [22]: HM, 0.025AT and 0.3AT were pretreated at 500 °C for 1 h and then cooled down to 350 °C under N_2 flow. Subsequently, the transformation of *m*-xylene (>99%, J&K) was carried out at 350 °C, atmospheric pressure and 13 h^{-1} of *m*-xylene WHSV with N_2 flow (32.5 ml/min) for 10 h. Samples with only sinusoidal pore accessible (named as $HM_{xy\text{-DMQ}}$, $0.025AT_{xy\text{-DMQ}}$ and $0.3AT_{xy\text{-DMQ}}$), for the IR characterization, were prepared by dropwise adding mixture of 2,4-dimethylquinoline (2,4-DMQ) (97%, TCI) and dichloromethane to the HM_{xy}, $0.025AT_{xy}$ and $0.3AT_{xy}$ wafers.

2.2. Characterization

X-ray diffraction (XRD) patterns were collected on an X Pert Pro X-ray diffractometer operated at 40 kV and 40 mA using Cu Kα radiation. The relative crystallinities (RC) of the samples were estimated by comparing the areas of their characteristic peaks (10.0°, 14.3°, 16.0°, 22.7° and 26.0° of 2θ) with those of 0.025AT, which was assumed as 100%.

$$\mathrm{RC} = \frac{\text{The area of characteristic peaks of the sample}}{\text{The area of characteristic peaks of 0.025AT}} \times 100\%$$

The chemical composition of samples was analyzed on a Philip Magix 601X X-ray fluorescence (XRF) spectrometer.

Ammonia temperature-programmed desorption (NH_3-TPD) was performed in a conventional U-shaped stainless steel micro-reactor (i.d. = 4 mm) with helium (He) as the carrier gas. The effluent was monitored by an online gas chromatograph (Shimadzu GC-8A) equipped with a TCD detector. Typically, the sample (0.14 g) was pretreated at 600 °C for 1 h, then cooled down to 150 °C and saturated with NH_3. After a stable baseline had been obtained, the sample was heated from 150 to 600 °C at a ramp rate of 18.8 °C/min.

The stability of the coke generated in the transformation of *m*-xylene was analyzed by the thermogravimetry and differential scanning calorimetry (TG-DSC) analysis with a Netzsch STA 449F3-DSC 204HP analyzer. The process was performed from 40 to 400 °C at a ramp rate of 10 °C/min under N_2 flow. The effluent was analyzed by an Ametek Dymaxion mass spectrometer (MS).

N_2 adsorption was carried out at −196 °C with an automatic Micromeritics ASAP 2020 apparatus. The fresh samples were pretreated under vacuum at 350 °C for 6 h. However, the precoked samples were pretreated only at 100 °C for 2 h to prevent coke from being removed [22].

The Brönsted (B) and Lewis (L) acid sites of samples were determined by pyridine adsorption followed by infrared (Py-IR) measurements on a Bruker 70 IR spectrometer. Samples were pressed into self-supported wafers, followed by evacuation at 250 °C for 2 h (1×10^{-2} Pa) in IR cell. After the sample was cooled down to the room temperature, a spectrum was recorded as background. Subsequently, the wafers were exposed to pyridine vapor for 20 min at 0 °C and then outgassed at 150 °C for 30 min. The spectra were collected at room temperature. The distributions of B and L acid sites in three pore systems of HM, 0.025AT and 0.3AT were determined by a subtraction method with the bands at 1543 and 1450 cm^{-1} using the values of the molar extinction coefficients (1.13 and 1.28 cm μmol^{-1}) determined by Guisnet [23]. For example, in sample HM, the amounts of B and L acid sites in sinusoidal pores were calculated with the integrated spectrum of $HM_{xy\text{-DMQ}}$, and the distribution of B and L acid sites in the surface pockets and supercages was acquired by the difference in results between HM_{xy} and $HM_{xy\text{-DMQ}}$ and between HM and HM_{xy}, respectively. The OH stretching spectra were determined after activating the samples in situ in an IR cell in vacuum (1×10^{-3} Pa) at 250 °C for 5 h.

2.3. Catalyst evaluation

Liquid alkylation of benzene (>99%, J&K) with ethylene was carried out in a stainless steel fixed bed reactor. One gram of catalyst was loaded in the center of the reactor and pretreated at 500 °C for 1 h in N_2. After the reactor was cooled down to 220 °C, benzene was pumped in to fully fill the reactor before ethylene was introduced. The reactions were carried out at 3.5 MPa, 220 °C, 1.5 h^{-1} of weight hourly space velocity (WHSV) of ethylene, 12/1 of benzene/ethylene molar ratio. The samples with precoked supercages were washed in the liquid benzene (300 ml h^{-1} g^{-1}) for 30 min to remove carbon on the surface of catalysts before ethylene was introduced. The sample with the precoked supercage and poisoned surface pockets, such as $HM_{xy\text{-DMQ}}$, was obtained by poisoning the external surface of HM_{xy} by means of 2,4-DMQ adsorption. The poisoning process was carried out by adding a given amount of 2,4-DMQ into benzene. When the liquid alkylation of benzene with ethylene was performed, the flow rate of 2,4-DMQ was 207 μmol·(g cat)$^{-1}$ h^{-1}. The ethylene conversion and selectivities of products within different pore systems were calculated using the same method as that in Section 2.2 for the distributions of B and L acid sites.

3. Results and discussion

3.1. Characterization of the precoked and poisoned samples

As shown in Fig. 1, HM possesses fully crystalline MWW structure [24]. After HM is precoked through *m*-xylene transformation

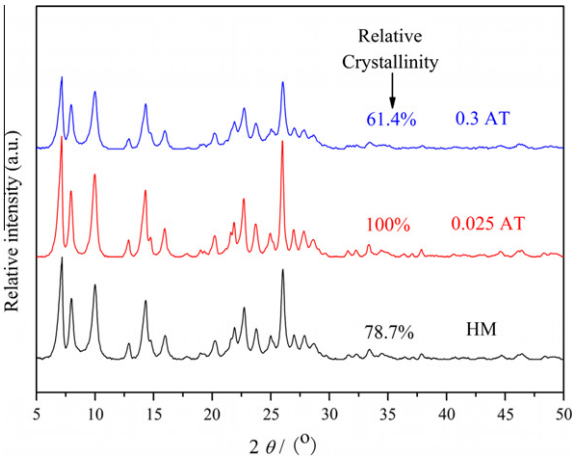

Fig. 1. XRD patterns of MCM-49 zeolite before and after alkali-treatment.

(HM_{xy}), the surface area reduces by 294 m^2/g, which is similar to its reduced area of micropore (263 m^2/g) (Table 1), indicating that most coke is located in micropores. The remaining micropore volume (0.053 m^3/g) of HM_{xy} is 31.2% of that in HM. This is perfectively in agreement with the molecular modeling results that the volume of the sinusoidal pores takes up 30% of the total micropore volume in MWW zeolites [25]. This result suggests that the supercages can be successfully blocked by the coke generated in the *m*-xylene transformation reaction while the sinusoidal pore is preserved.

The mass loss determined by TG curve below 200 °C (spectra are not shown here) is generally regarded as the evaporation of the adsorbed water and corresponds to the endothermic peak in the DSC curve. Moreover, the mass loss between 200 and 400 °C is not significant. No coke signal except N_2 and H_2O is detected by mass spectra in the temperature range of 40–400 °C, suggesting that coke located in the supercages is stable below 400 °C. 2,4-DMQ adsorption has been proved to be an effective method to poison the surface pockets of HMCM-22 zeolite. Furthermore, the physisorbed and hydrogen-bonded 2,4-DMQ can be eliminated over 200 °C [16]. So, the precoked and poisoned samples should be characterized under proper conditions.

Fig. 2 shows the FT-IR spectra of HM, HM_{xy} and $HM_{xy\text{-}DMQ}$ in the –OH stretching region (3800–3500 cm^{-1}). Four –OH bands are observed in the spectrum of HM. The bands at about 3745 and 3722 cm^{-1} are related with the external and the internal silanol groups, respectively. The band at 3618 cm^{-1} is attributed to bridging hydroxyl groups. Another band at 3668 cm^{-1} is ascribed to Al–OH groups, where Al is connected with the zeolite framework by one or two chemical bonds [26,27]. For the precoked sample (HM_{xy}), the band at 3668 cm^{-1} is hardly to be observed, indicating that most extraframework aluminum species are located in the supercages. The band of external silanol group seems not to be affected by coke, but that of the internal silanol group shifts to the lower wave number region (~3712 cm^{-1}) with a weaker intensity. This is possibly caused by the interaction between the silanol groups and the coke in the supercages. The band intensity of bridging hydroxyl groups also obviously decreases, which is consistent with the results on MCM-22 catalysts obtained by Matias et al. [2]. This indicates that the bridging hydroxyl groups and the extraframework aluminum species in the supercages, which are widely regarded as the origin of B and L acid sites, have been covered by coke generated in the *m*-xylene transformation reaction. Compared with HM_{xy}, $HM_{xy\text{-}DMQ}$ exhibits much lower band intensity at ~3745 cm^{-1}, and this is in agreement with the results of Ayrault et al. [16]. It confirms that 2,4-DMQ can effectively poison the active sites in the pockets of HM_{xy}.

The acid properties of MCM-49 samples were studied by Py-IR and NH_3-TPD techniques. In the Py-IR spectra (Fig. 3), the bands at 1450 and 1543 cm^{-1} are representative of L and B acid sites, respectively [28,29]. The band at 1490 cm^{-1} is related with both L and B acid sites. Compared with HM, the band intensity at 1450 cm^{-1} of HM_{xy} exhibits a much more notable decrease than the one at 1543 cm^{-1}, indicating that the percentage of L acid sites is higher than that of B acid sites in the supercages. The distribution of L and B acid sites in different pores of HM is calculated with Py-IR spectra of HM, HM_{xy} and $HM_{xy\text{-}DMQ}$ and the results are listed in Table 2. The data clearly show that most L acid sites (ca. 73%) are located in the supercages in HM, while 34% of B acid sites are located in the supercages, 38% in the pockets and 28% in the sinusoidal pores.

Table 1
N_2 adsorption and desorption results of fresh and coked MCM-49 before and after alkali-treatment.

	S_{BET} (m^2/g)	S_{micro} (m^2/g)	V_{total} (cm^3/g)	V_{micro} (cm^3/g)
HM	486	378	0.49	0.17
HM_{xy}	192 (−294)	115 (−263)	0.39	0.05
0.025AT	458	348	0.42	0.17
$0.025AT_{xy}$	197 (−261)	118 (−230)	0.33	0.05
0.3AT	442	284	0.55	0.13
$0.3AT_{xy}$	194 (−248)	114 (−170)	0.42	0.05

Data listed within the parenthesis are the decreased value of the precoked sample when compared with the fresh sample.

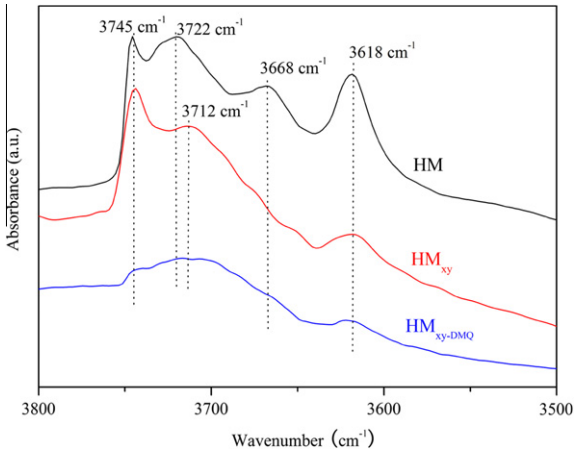

Fig. 2. The FT-IR spectra of HM, HM_{xy} and $HM_{xy\text{-}DMQ}$ in the –OH stretching region. HM: H-type MCM-49 zeolite. HM_{xy}: H-type MCM-49 zeolite with the blocked supercage. $HM_{xy\text{-}DMQ}$: H-type MCM-49 zeolite with the blocked supercage and poisoned surface pockets.

3.2. Roles of acid sites in different pores of MCM-49 for catalytic ethylene conversion

As shown in Fig. 4A, ethylene conversion exhibits a very fast decrease at the early period over HM and then tends to be stable. In comparison, within 12 h of time on stream (TOS), ethylene conversion is stable at about 70% and 8% over HM_{xy} and $HM_{xy\text{-}DMQ}$, respectively. Since the supercages of HM_{xy} are blocked, and both the supercages and the surface pockets of $HM_{xy\text{-}DMQ}$ are poisoned, ethylene conversion within different pores vs. TOS can be obtained from Fig. 4A. As shown in Fig. 4B, there is not obvious decrease for ethylene conversion within the surface pockets and sinusoidal pores during the TOS investigated. At TOS of 1 h, 26.2% of ethylene is converted in the supercages, and it decreases gradually to only

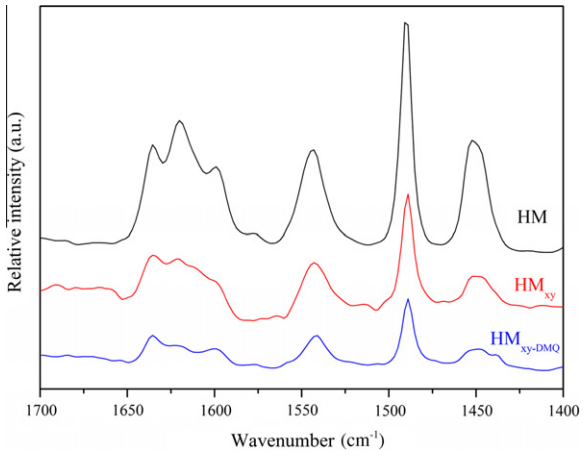

Fig. 3. IR spectra of pyridine adsorbed HM, HM_{xy} and $HM_{xy\text{-}DMQ}$.

Table 2
Calculated distributions of B and L acid sites, ethylbenzene, diethylbenzene and C_{10}+ aromatics yields in different pores of HMCM-49.

	Supercage	Pocket	Sinusoidal
B (%)	34	38	28
L (%)	73	10	17
Ethylbenzene (%)	19.5	72.5	8.0
Diethylbenzene (%)	40.7	54.9	4.4
C_{10}+ aromatics (%)	80.4	19.5	0.1

Reaction conditions: 3.5 MPa, 220 °C, 12 of B/E molar ratio, 1.5 h^{-1} of WHSV (ethylene), 3 h of TOS.

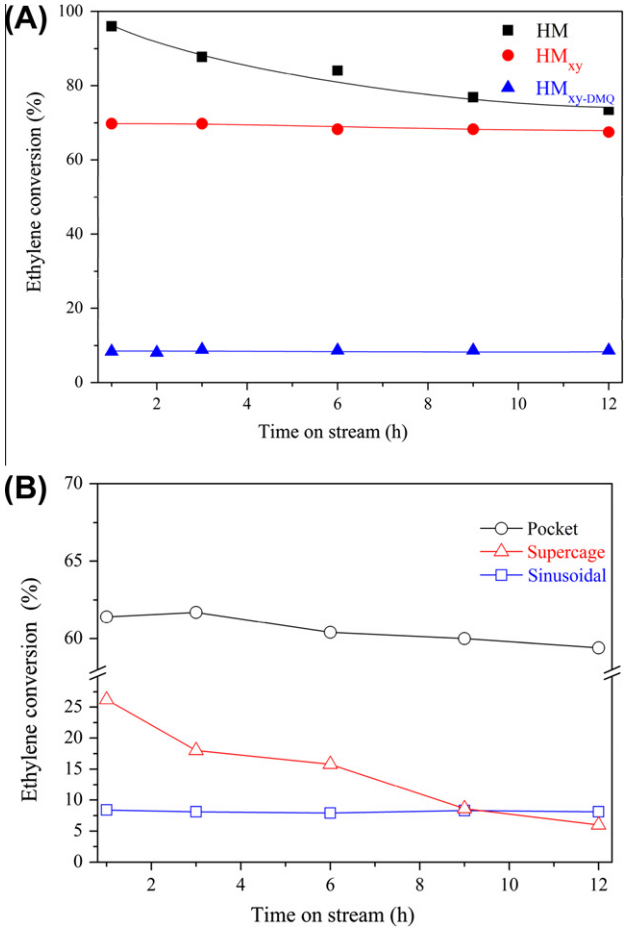

Fig. 4. (A) Ethylene conversion vs. time on stream over HM, HM_{xy} and $HM_{xy\text{-}DMQ}$. (B) Ethylene conversion vs. time on stream in different pores of HM. Reaction conditions: 3.5 MPa, 220 °C, 12 of B/E molar ratio and 1.5 h^{-1} of WHSV (ethylene).

6% at TOS of 12 h. Accordingly, the overall conversion of ethylene over HM decreases from 96% (TOS = 1 h) to 73.5% (TOS = 12 h). Therefore, the deactivation mainly takes place in the supercages of HM.

Fast decrease in conversion at the early reaction stage is also observed over MCM-22 zoelite when it is applied in xylene isomerization [17], *n*-heptane cracking [30], toluene disproportionation [8,31], methylcyclohexane transformation [2], alkylation reaction [32] and butane isomerization [33]. Matias et al. attributed the fast deactivation of the methylcyclohexane transformation over MCM-22 to the formation of coke in the supercages [2]. Corma et al. suggested that the fast decrease in strong acid sites resulted in the deactivation of MCM-22 zeolite catalysts in the alkylation of isobutane and 2-butene [32]. According to the theoretical modeling by Sastre [34], the acid sites located within the supercages tend to be relatively strong. Additionally, Li et al. found that more oligomer products and coke were produced with the increase in L acid sites by comparing the parent with the hydrothermally treated MCM-22 zeolites in the alkylation of benzene with diethyl carbonate [35]. Since most L acid sites are located within the supercages of HM (Table 2), the oligomerization and coking reaction of ethylene will cover some of strong acid sites, resulting in the deactivation of HM. In addition, when zeolites are synthesized or post-treated, the non-crystalline raw materials or amorphous silica–alumina generated in the calcination process is usually included [36–38]. These amorphous silica–alumina species might deposit on the surface of MCM-49 zeolite and cause partial blockage of the 10MR opening of the supercages [39]. The resulting hindrance for the diffusion of the bulky by-product molecules might also cause deactivation of the supercages.

Liquid alkylation of benzene with ethylene was mainly catalyzed by strong acid sites, while weak acid sites were almost ineffective for the reaction [7]. Therefore, it is understandable for the low ethylene conversion within the sinusoidal pores (most acid sites are relatively weak) of MCM-49 [34].

3.3. Distribution of products in different pores of MCM-49

Liquid alkylation of benzene with ethylene is a complicated process, which mainly includes the following reaction routes: alkylation between ethylene and benzene produces ethylbenzene (process A), further alkylation of ethylbenzene with ethylene generates diethyl- or polyethylbenzene [11,40] (process B), oligomerization of ethylene [41,42] (process C) and the transformation of alkylbenzene (polyethylbenzene or products of alkylation between benzene with ethylene oligomers) (process D) yield molecule with bigger size [19].

Within 12 h of TOS, the distribution of products over HM, HM_{xy} and $HM_{xy\text{-}DMQ}$ exhibits indistinctive change. The yields of the representative products, ethylbenzene, C_{10}+ aromatics (heavy aromatic products with ten and more carbon atoms) and diethylbenzene within different pore systems of HM can be calculated with the values at 3 h of TOS in Table 3. The yield of ethylbenzene in the supercages and in the sinusoidal pores is much lower than that in the surface pockets (Table 2). Moreover, more than half of diethylbenzene is yielded in the pockets, indicating that the surface pockets are the main locations for the alkylation of benzene (processes A and B). Additionally, the yield of C_{10}+ aromatics in the supercages is the highest among these in three different pore systems (process D).

Since the supercage in MCM-49 zeolite has large internal space and a relatively small 10MR opening, it facilitates the reactions that produce relatively large molecules, such as processes B and D. Compared with the smaller molecule like ethylbenzene, the

Table 3
The selectivities of products in the alkylation of benzene with ethylene over different samples.

Catalysts	HM	HM_{xy}	$HM_{xy\text{-}DMQ}$	0.3AT	0.025AT
Ethylene conversion (mol%)	87.8	69.8	8.1	92.1	97.2
Product selectivity (mol%)					
Ethylbenzene	96.4	97.5	84.1	96.0	96.2
m-Diethylbenzene	0.8	0.6	0.2	1.2	1.1
p-Diethylbenzene	0.9	0.6	1.1	0.9	0.9
o-Diethylbenzene	1.1	0.9	0.1	1.4	1.1
Toluene	0.09	0.14	5.40	0.09	0.13
C_9 aromatics	0.06	0.02	0	0.04	0.07
C_{10}+ aromatics	0.57	0.14	<0.01	0.27	0.41
Paraffins	0.08	0.10	9.10	0.10	0.09

Reaction conditions: 3.5 MPa, 220 °C, 12 of B/E molar ratio, 1.5 h^{-1} of WHSV (ethylene), 3 h of TOS.

diffusion of heavy aromatic products out of the supercages is significantly inhibited. Simultaneously, as the alkylbenzene has higher electronegativity than benzene molecule, further alkylation of alkylbenzene with carbocations (process B) will happen if the space in the pore is large enough. Furthermore, cracking, cyclization and transformation of alkylbenzene will produce aromatics with condensed rings and block the supercages [19,22] (process D). In contrast, ethylbenzene produced in the surface pockets would readily diffuse out due to its limited diffusion constraints, and further reactions could be inhibited.

In the sinusoidal pores, the relatively weak acid sites [34] and narrow channel do not favor the processes A, B and D that need strong acid sites [7] or produce molecules with bigger size. $HM_{xy\text{-}DMQ}$ with only sinusoidal pore accessible shows lower selectivities toward ethylation products and only trace quantity of C_{10}+ is detected (Table 3). The small amount of diethylbenzene produced in sinusoidal pores is predominantly *para*-product. However, the formation of paraffin by oligomerization of ethylene (process C) and toluene by paring of ethylbenzene (process E) are slow involving relatively complex mechanisms. Compared with supercage and pocket, the zigzag and longer channel of sinusoidal pore is a more proper location for these kinds of reactions. Moreover, these two reactions can be effectively catalyzed by relatively weak acid sites [43,44], so the selectivities of toluene and paraffin (Table 3) on $HM_{xy\text{-}DMQ}$ are distinctively higher than those over HM and HM_{xy}.

In conclusion, the generation of ethylbenzene mainly occurs in the surface pockets, and heavy aromatics produced in the supercages are responsible for the deactivation of MCM-49 zeolite. Few opportunities for the alkylation reactions within the sinusoidal pores can be attributed to the lack of strong acid sites and the space restriction inside those small pores.

3.4. Effects of the alkali treatment on different pore systems of MCM-49 zeolite

Recently, the alkali treatment was found to be an effective method to enhance catalytic performance of MCM-49 zeolite in liquid alkylation of benzene with ethylene [45]. Herein, the reasons for this will be elucidated in more detail with the methods mentioned in Section 3.1.

It has been reported that the RC of zeolite can be effectively improved with the mild alkali-treatment conditions [38] and then decreases with harsh treatment conditions [46,47]. We also observe a similar phenomenon. For example, the RC increases from 78.7% for HM to 100% for 0.025AT and then decreases to 61.4% for 0.3AT (Fig. 1). Due to the extraction of Si atoms from the framework of zeolites, the Si/Al molar ratio decreases from 10.2 for HM to 7.9 for 0.3AT [48,49].

The effect of the alkali treatment on the distribution of acid sites within different pore systems of the MCM-49 zeolite is also investigated. As seen from Table 4, the ratio between the amount of B acid site in the surface pockets and in the supercages ($B_{(poc/sup)}$) increases over samples upon alkali treatment under more harsh conditions. According to the results before [45], the opening of supercages can be expanded by selectively extracting Si atoms on T1 and T3 sites upon alkali treatment in NaOH solution. Within expanded supercages, the diffusion of relatively large molecules in/out of the supercages is improved. Part of acid sites in the supercages will not be effectively covered by the precoking process and will be regarded as the acid sites similar to those in the surface pockets, resulting in an increased $B_{(poc/sup)}$. In a word, the alkali-treatment process introduces some pores similar to the surface pockets, which is much favorable for the alkylation of benzene with ethylene. However, the proportion of B acid sites in the sinusoidal pores exhibits little change under different alkali-treatment conditions (Table 4), indicating that the alkali treatment has less significant influence on the acid sites within the sinusoidal pores.

As shown in Fig. 5, bands related to the stretching vibration of Al–OH (3668 cm^{-1}) and bridging hydroxyl groups (3618 cm^{-1}) show little change over 0.3AT. On the other hand, the intensity of peak at 3745 cm^{-1}, corresponding to the external Si–OH, increases sharply upon more harsh conditions. This could be attributed to the breakage of Si–O–Si bonds in basic solution [45]. Another interesting observation is that $0.025AT_{xy}$ and $0.3AT_{xy}$ show similar V_{micro} as HM_{xy}, and this V_{micro} nearly equals to the volume of the sinusoidal pores in the parent MCM-49 zeolite (Table 1), suggesting that the destroyed micropores in NaOH solutions are mainly the supercages, and the structure of sinusoidal pores is preserved.

Fig. 4B shows that ethylene conversion within the surface pockets and sinusoidal pores of HM is stable with TOS. Similar results are also observed over 0.025AT and 0.3AT. Ethylene conversion within the supercages of HM, 0.025AT and 0.3AT reduces by 31.3%, 12.1% and 22.5% with TOS from 1 to 3 h, respectively (Table 4). These results suggest that alkali treatment can prevent the supercages in MCM-49 zeolite from deactivation.

In liquid alkylation of benzene with ethylene, the coke content can be estimated from the change of pore volume by N_2 adsorption measurement (Table 4) [50,51]. Apart from the micropores consist-

Table 4
The distribution of ethylene conversion, B acid sites in different channels, $B_{(poc/sup)}$, Si/Al molar ratio, amount of acid and amount of coke over HM, 0.025AT and 0.3AT.

Catalysts	Pore	Eth. con. (%)		B[a] (%)	$B_{(poc/sup)}$	Si/Al[b] (molar ratio)	Acid amount[c] (mmol/g)	$Coke_{total}$[d] (cm^3/g Catalyst)	$Coke_{micro}$[d] (cm^3/g Catalyst)
		1 (h)	3 (h)						
HM	Supercage	26.2	18.0 (31.3%)	34					
	Pocket	61.4	61.7 (−0.5%)	38	1.12	10.2	0.79	0.18	0.13
	Sinusoidal	8.4	8.1 (3.6%)	28					
0.025AT	Supercage	21.5	18.9 (12.1%)	29					
	Pocket	69.8	70.1 (−0.4%)	44	1.52	10.5	0.79	0.17	0.14
	Sinusoidal	8.5	8.2(3.5%)	27					
0.3AT	Supercage	24.4	18.9 (22.5%)	25					
	Pocket	63.6	63.9 (0.5%)	48	1.92	7.9	0.80	0.11	0.08
	Sinusoidal	9.7	9.3 (4.1%)	27					

Data listed within the parenthesis are the decreased percent of ethylene conversion at the TOS of 3 h when compared with the value at 1 h of TOS.
$B_{(poc/sup)}$: the ratio of B acid site located in the surface pockets and in the supercages.
Reaction conditions: 3.5 MPa, 220 °C, 12 of B/E molar ratio, 1.5 h^{-1} of WHSV (ethylene).
[a] B acid site distribution, measured by Py-IR.
[b] Measured by XRF.
[c] Measured by NH_3-TPD.
[d] Amount of coke (generated in the liquid alkylation reaction) measured by N_2 adsorption ($Coke_{total}$: the total amount of coke over samples, $Coke_{micro}$: coke located within the micropores).

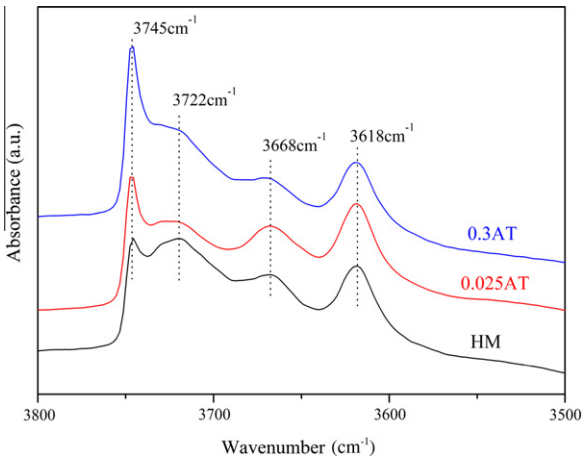

Fig. 5. The FT-IR spectra of HM, 0.025AT and 0.3AT in the –OH stretching region. HM: H-type MCM-49 zeolite. 0.025AT: H-type MCM-49 zeolite alkali-treated in 0.025 N NaOH solution for 15 min at the room temperature. 0.3AT: H-type MCM-49 zeolite alkali-treated in 0.3 N NaOH solution for 120 min at 75 °C.

ing of sinusoidal pores and supercages in MCM-49 zeolite, there are also mesopores originating from the aggregation of MCM-49 sheets and extra mesopores introduced in alkali treatment with certain NaOH solutions. After liquid alkylation of benzene with ethylene for 12 h, compared with HM, the total coke content of 0.025AT exhibits limited change, and only the proportion of coke deposited in micropores is a bit higher. The amount of coke over 0.3AT, especially that in micropores, is obviously lower than that over HM. Moreover, the selectivities of most products with relatively small molecule size are not influenced by the alkali-treatment process (Table 3), but the selectivity of C_{10}+ aromatics decreases from 0.57% over HM to only 0.27% over 0.3AT. Since the mild alkali-treatment process can destroy part of aggregated mesopores, the coke deposit in the mesopores of 0.025AT decreases, accompanying with the increase in coke deposition in micropores. Over 0.3AT, the diffusion condition is improved with the introduction of mesopores by alkali-treatment, and the diffusion path in the micropores is shortened by desilication [52–54]. Reactions that produce larger molecules such as processes B and D will be inhibited, resulting in the decrease in the C_{10}+ aromatics as well as coke deposition in micropores. In conclusion, alkali treatment is an efficient method to improve the catalytic performances of MCM-49 zeolite by introducing mesopores into the zeolite, as well as expanding the opening of the supercages.

4. Conclusions

Through two-step process of precoking and 2, 4-DMQ adsorption, distributions of acid sites in three different types of pore systems of MCM-49 zeolite have been determined. The ratio of B acid sites in the surface pockets, in the supercages and in the sinusoidal pores is about 1.4:1.2:1.0. Most L acid sites (ca. 73%) exist within supercages.

Under the selected conditions for the liquid alkylation of benzene with ethylene, more than 60% of ethylene conversion occurs in the surface pockets, and less than 30% and 10% takes place in the supercages and the sinusoidal pores, respectively. The roles of pores have been proposed. The surface pockets are the main positions for ethylbenzene production, and they also yield more than half of diethylbenzene. The majority of C_{10}+ aromatics are produced in the supercages, and coke deposition within the supercages is the main reason for the fast deactivation of MCM-49 zeolite at the early reaction stage. The sinusoidal system has a little contribution to the production of ethylation products, but it is favorable to the oligomerization of ethylene.

Further studies show that the catalytic performance of MCM-49 zeolite for liquid alkylation of benzene with ethylene can effectively improved by moderate alkali treatment due to the generation of some pores resembling the surface pockets.

Acknowledgment

We acknowledge the National Basic Research Program of China (No. 2009CB623501) for financial support.

References

[1] C. Perego, P. Ingallina, Catal. Today 73 (2002) 3.
[2] P. Matias, J.M. Lopes, S. Laforge, P. Magnoux, P.A. Russo, M.M.L. Ribeiro Carrott, M. Guisnet, F. Ramôa Ribeiro, J. Catal. 259 (2008) 190.
[3] J. Rigoreau, S. Laforge, N. Gnep, M. Guisnet, J. Catal. 236 (2005) 45.
[4] B. Onida, F. Geobaldo, F. Testa, F. Crea, E. Garrone, Micropor. Mesopor. Mater. 30 (1999) 119.
[5] D. Meloni, S. Laforge, D. Martin, M. Guisnet, E. Rombi, V. Solinas, Appl. Catal. A: Gen. 215 (2001) 55.
[6] G.G. Juttu, R.F. Lobo, Micropor. Mesopor. Mater. 40 (2000) 9.
[7] X.D. Sun, Q.X. Wang, L.Y. Xu, S.L. Liu, Catal. Lett. 94 (2004) 75.
[8] P. Wu, T. Komatsu, T. Yashima, Micropor. Mesopor. Mater. 22 (1998) 343.
[9] A. Corma, V. Martínez-Soriab, E. Schnoevelda, J. Catal. 192 (2000) 163.
[10] J. Cheng, T. Degnan, J. Beck, Y. Huang, M. Kalyanaraman, J. Kowalski, C. Loehr, D. Mazzone, Stud. Surf. Sci. Catal. 121 (1999) 53.
[11] G. Bellussi, G. Pazzuconi, C. Perego, G. Girotti, G. Terzoni, J. Catal. 157 (1995) 227.
[12] S. Lawton, M. Leonowicz, R. Partridge, P. Chu, M. Rubin, Micropor. Mesopor. Mater. 23 (1998) 109.
[13] A. Corma, C. Corell, J. Pérez-Pariente, Zeolites 15 (1995) 2.
[14] A. Corma, V. Fornés, L. Forni, F. Márquez, J. Martínez-Triguero, D. Moscotti, J. Catal. 179 (1998) 451.
[15] H. Du, D. Olson, J. Phys. Chem. B 106 (2002) 395.
[16] P. Ayrault, J. Datka, S. Laforge, D. Martin, M. Guisnet, J. Phys. Chem. B 108 (2004) 13755.
[17] S. Laforge, D. Martin, M. Guisnet, Appl. Catal. A: Gen. 268 (2004) 33.
[18] S. Laforge, D. Martin, M. Guisnet, Micropor. Mesopor. Mater. 67 (2004) 235.
[19] S. Laforge, D. Martin, J.L. Paillaud, M. Guisnet, J. Catal. 220 (2003) 92.
[20] S. Lawton, A. Fung, G. Kennedy, L. Alemany, C. Chang, G. Hatzikos, D. Lissy, M. Rubin, H. Timken, S. Steuernagel, J. Phys. Chem. 100 (1996) 3788.
[21] J. Cheng, C. Smith, D. Walsh, US Patent 5493065, 1996 (to Mobil Oil Corporation).
[22] P. Matias, J. Lopes, S. Laforge, P. Magnoux, M. Guisnet, F. Ramoa Ribeiro, Appl. Catal. A: Gen. 351 (2008) 174.
[23] M. Guisnet, P. Ayrault, C. Coutanceau, M. Fernanda Alvarez, J. Datka, J. Chem. Soc. Faraday Trans. 93 (1997) 1661.
[24] J.M. Bennett, C.D.Chang, S.L. Lawton, M.E., Leonowicz, D.N. Lissy, M.K. Rubin, B. Cynwyd, US Patent 5236575, 1993 (to Mobil Oil Corporation).
[25] E. Besset, D. Meloni, D. Martin, M. Guisnet, L. Schreyeck. In: B. Delmon, G.F. Froment (Eds.), Catalyst Deactivation 1999, Proc. 8th Int. Symp., 10–13 October 1999, vol. 126, p. 171.
[26] A. Corma, C. Corell, V. Fornés, W. Kolodziejski, J. Pérez-Pariente, Zeolites 15 (1995) 576.
[27] M. Maache, A. Janin, J.C. Lavalley, J.F. Joly, E. Benazzi, Zeolites 13 (1993) 419.
[28] E.P. Parry, J. Catal. 2 (1963) 371.
[29] K. Song, J. Guan, S. Wu, Y. Yang, B. Liu, Q. Kan, Catal. Lett. 126 (2008) 8.
[30] D. Meloni, D. Martin, M. Guisnet, Appl. Catal. A: Gen. 215 (2001) 67.
[31] X. Ren, J. Liang, J. Wang, J. Porous Mater. 13 (2006) 353.
[32] A. Corma, A. Martinez, C. Martinez, Catal. Lett. 28 (1994) 187.
[33] H.J. Jung, S.S. Park, C.H. Shin, Y.K. Park, S.B. Hong, J. Catal. 245 (2007) 65.
[34] G. Sastre, V. Fornes, A. Corma, J. Phys. Chem. B 104 (2000) 4349.
[35] Y. Li, B. Xue, X. He, J. Mol. Catal. A: Chem. 301 (2009) 106.
[36] A. Albuquerque, L. Marchese, L. Lisi, H.O. Pastore, J. Catal. 241 (2006) 367.
[37] A. Corma, A. Martinez, C. Martinez, Appl. Catal. A: Gen. 134 (1996) 169.
[38] E. Roland, P. Kleinschmit, A. Kiss, F. Heindl, US Patent 5223240, 1993, (to Degussa Aktiengesellschaft, Fed. Rep. of Germany).
[39] H. Darmstadt, C. Roy, S. Kaliaguine, T. Kim, R. Ryoo, Chem. Mater. 15 (2003) 3300.
[40] A. Geatti, M. Lenarda, L. Storaro, R. Ganzerla, M. Perissinotto, J. Mol. Catal. A: Chem. 121 (1997) 111.
[41] J.P. Lange, A. Gutsze, J. Allgeier, H.G. Karge, Appl. Catal. 45 (1988) 345.
[42] K.A. Becker, H.G. Karge, W.D. Streubel, J. Catal. 28 (1973) 403.
[43] A. Feller, I. Zuazo, A. Guzman, J.O. Barth, J.A. Lercher, J. Catal. 216 (2003) 313.
[44] P.D. Hopkins, J. Catal. 12 (1968) 325.
[45] K. Liu, S. Xie, G. Xu, Y. Li, S. Liu, L. Xu, Appl. Catal. A: Gen. 383 (2010) 102.
[46] L. Mokrzycki, B. Sulikowski, Z. Olejniczak, Catal. Lett. 127 (2009) 296.
[47] L.L. Su, L. Liu, J.Q. Zhang, H.X. Wang, Y.G. Li, W.J. Shen, Y.D. Xu, X.H. Bao, Catal. Lett. 91 (2003) 155.
[48] Y. Tao, H. Kanoh, L. Abrams, K. Kaneko, Chem. Rev. 106 (2006) 896.

[49] X. Wei, P.G. Smirniotis, Micropor. Mesopor. Mater. 97 (2006) 97.
[50] D.M. Bibby, N.B. Milestone, J.E. Patterson, L.P. Aldridge, J. Catal. 97 (1986) 493.
[51] J. Kim, M. Choi, R. Ryoo, J. Catal. 269 (2010) 219.
[52] J.C. Groen, J.A. Moulijn, J. Pérez-Ramírez, Micropor. Mesopor. Mater. 87 (2005) 153.
[53] J.C. Groen, W. Zhu, S. Brouwer, S.J. Huynink, F. Kapteijn, J.A. Moulijn, J. Pérez-Ramírez, J. Am. Chem. Soc. 129 (2007) 355.
[54] J.C. Groen, J.A. Moulijn, J. Pérez-Ramírez, J. Mater. Chem. 16 (2006) 2121.